

AD-787 790

ADVANCED ION SOURCE

Harry J. King

Hughes Research Laboratories

Prepared for:

Air Force Technical Applications Center  
Advanced Research Projects Agency

March 1974

DISTRIBUTED BY:

**NTIS**

National Technical Information Service  
U. S. DEPARTMENT OF COMMERCE

DOCUMENT CONTROL DATA - R&D		
<i>(Security classification of title, body of abstract and indexing annotation must be entered when the overall report is classified)</i>		
1. ORIGINATING ACTIVITY <i>(Corporate author)</i> Hughes Research Laboratories 3011 Malibu Canyon Road Malibu, California 90265		2a. REPORT SECURITY CLASSIFICATION Unclassified
		2b. GROUP
3. REPORT TITLE ADVANCED ION SOURCE (Phase II Report)		
4. DESCRIPTIVE NOTES <i>(Type of report and inclusive dates)</i> Phase II, Final Report 22 June 1973 through 24 January 1974		
5. AUTHOR(S) <i>(First name, middle initial, last name)</i> Harry J. King		
6. REPORT DATE March 1974	7a. TOTAL NO. OF PAGES 26 31	7b. NO. OF REFS 2
8a. CONTRACT OR GRANT NO. F08606-73-C-0038	9a. ORIGINATOR'S REPORT NUMBER(S) Phase II	
b. PROJECT, TASK, WORK UNIT NOS. 3F10		
c. DOD ELEMENT	9b. OTHER REPORT NO(S) <i>(Any other numbers that may be assigned this report)</i>	
d. DOD SUBELEMENT		
10. DISTRIBUTION STATEMENT Distribution unlimited.		
11. SUPPLEMENTARY NOTES N/A	12. SPONSORING MILITARY ACTIVITY Advanced Research Projects Agency	
13. ABSTRACT  The experiments conducted during Phase II of this program have determined that cesium and iodine ion source brightnesses of 60 and 70 A/cm <sup>2</sup> sr, respectively, have been obtained. Increasing these values to 200 A/cm <sup>2</sup> sr for the cesium ion source and to 100 A/cm <sup>2</sup> sr for the iodine source appears feasible. Operation of the prototype system has provided the parametric operating data and design experience necessary to construct the deliverable hardware.		

Reproduced by  
NATIONAL TECHNICAL  
INFORMATION SERVICE  
U S Department of Commerce  
Springfield VA 22151

UNCLASSIFIED  
Security Classification

14. KEY WORDS	LINK A		LINK B		LINK C	
	ROLE	WT	ROLE	WT	ROLE	WT
Cesium ion beam						
Iodine ion beam						
Positive ions						
Negative ions						
Contact ionization						
Ion optics						
Ion beam brightness						

ia

UNCLASSIFIED  
Security Classification



ADVANCED ION SOURCE

Phase II Report

Project Scientist: H. King  
213-456-6411

Sponsored by  
Advanced Research Projects Agency  
ARPA Order No. 1702, Amd 3

AFTAC Project Authorization No. VT/3423/-/ETR  
Program Code No. 3F10  
Contract No. F08606-73-C-0038  
Effective: 21 March 1973  
Expiration: 24 January 1974  
Amount: \$219,780.00

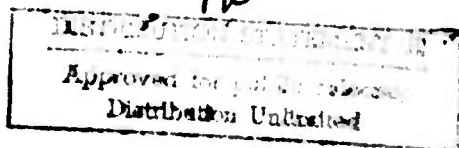
DDC  
RECEIVED  
OCT 29 1974  
RECEIVED

Project Officer: Capt. John P. Oss  
HQ USAF (AFTAC/TRE)  
Patrick Air Force Base, Florida 32925  
305-494-2822

This research was supported by the Advanced Research Projects Agency of the Department of Defense, and was monitored by HQ USAF (AFTAC/TD-4C), Patrick Air Force Base, Florida 32925 under Contract No. F08606-73-C-0038.

The views and conclusions contained in this document are those of the authors and should not be interpreted as necessarily representing the official policies, either expressed or implied, of the Advanced Research Projects Agency, the Air Force Technical Applications Center, or the U.S. Government.

DISTRIBUTION UNLIMITED



ABSTRACT

The experiments conducted during Phase II of this program have determined that cesium and iodine ion source brightnesses of 60 and 70 A/cm<sup>2</sup> sr, respectively, have been obtained. Increasing these values to 200 A/cm<sup>2</sup> sr for the cesium ion source and to 100 A/cm<sup>2</sup> sr for the iodine source appears feasible. Operation of the prototype system has provided the parametric operating data and design experience necessary to construct the deliverable hardware.

LIST OF CONTRIBUTORS

Project Scientist	H. J. King
Cesium Ion Source	J. W. Ward
Iodine Ion Source	D. E. Zuccaro
Mechanical Design	D. E. Schnellker

TABLE OF CONTENTS

	LIST OF ILLUSTRATIONS . . . . .	v
I.	INTRODUCTION . . . . .	1
II.	PROGRAM OUTLINE . . . . .	2
III.	ADVANCED ION SOURCE DEVELOPMENT . . . . .	3
	A. Cesium Ion Source . . . . .	3
	B. Iodine Ion Source . . . . .	14
	C. System Design . . . . .	21
IV.	CONCLUSION AND SUMMARY . . . . .	23
	REFERENCES . . . . .	24

## LIST OF ILLUSTRATIONS

Fig. 1.	Schematic of circuit diagram used for testing cesium ion source . . . . .	5
Fig. 2.	Theoretical ion perveance line and experimental points . . . . .	6
Fig. 3.	Computer calculated trajectories for Pierce extraction geometry . . . . .	8
Fig. 4.	Schematic of experimental arrangement used for making brightness measurements . . . . .	10
Fig. 5.	Schematic showing how beam brightness is calculated from measured parameters . . . . .	10
Fig. 6.	Measured brightness values as a function of beam voltage . . . . .	12
Fig. 7.	Change in tungsten work function as a function of arrival rate for different metals . . . . .	15
Fig. 8.	Cross-sectional view of negative ion system . . . . .	17
Fig. 9.	Pictorial schematic of negative ion system . . . . .	18
Fig. 10.	Plot of negative ion current as a function of the reciprocal temperature of the emitter . . . . .	20
Fig. 11.	Plot of electron to ion ratio values as a function of emitter temperature . . .	22

## I. INTRODUCTION

The Advanced Ion Source (AIS) with which the report deals will be a major subsystem of the Advance Mass Separator (AMS) currently under development by AFTAC. This AMS will serve as an exceedingly high resolution analyzer to determine the composition of surface layers or small particles. It accomplishes this analysis by mass analyzing the ions which are sputtered from the sample surface by a highly focussed ion beam. It has been demonstrated that incident ions of both electro-positive and electronegative species (here  $Cs^+$  and  $I^-$ ) are required to provide adequate sensitivity over the whole periodic table. Clearly, the more intense the incident ion beam the faster the analysis may be accomplished. Therefore, the goal of the present project (i. e., to provide a bright, stable source of  $Cs^+$  and  $I^-$ ) directly affects the speed and resolution of the instrument.

## II. PROGRAM OUTLINE

The program to develop the AIS has been divided into four phases:

Phase I - Design Study

Phase II - Prototype Hardware Development

Phase III - Deliverable Hardware Fabrication and  
Verification

Phase IV - Integration at AMS Facility.

This report is a summary of the Phase II results.

### III. ADVANCED ION SOURCE DEVELOPMENT

The two ion sources (i. e.,  $\text{Cs}^+$  and  $\text{I}^-$ ) are of similar mechanical and ion optical design permitting many common parts to be used in the two structures. The construction of the sources and their experimental evaluation were carried on as two parallel programs in order to shorten the development time and to provide the maximum flexibility in the development program.

Each ion source program had its own individual goals. The positive cesium source program, which was based on well demonstrated physical phenomena,<sup>1</sup> was designed primarily to demonstrate the accuracy of the ion optical design, and the ability to generate a beam of adequate brightness. The negative iodine source program was of a more fundamental nature with the goal of parametrically characterizing the ionization of iodine on a lanthanum hexaboride surface. These results are reported below.

#### A. Cesium Ion Source

##### 1. Design

The initial tests utilized the mechanical design described in the Phase I summary report.<sup>2</sup> These first tests demonstrated the ability to sustain the required operating voltage (20 kV) and to reach an ionizer operating temperature of 1200°C. However, when cesium was introduced it was found that spurious breakdowns occurred on the insulator surfaces above 9 kV. A design modification was made to the ion source in which the insulators were mounted completely to the rear of the ionizer mounting flange, and shielded by deep cylinders which prevented any line of sight cesium condensation from the ion source. This design allowed operation at 20 kV with cesium present, with negligible insulator leakage currents. This design was used for all the subsequent tests which are described below.

## 2. Operation

A schematic of the circuit diagram used for testing the cesium ion source is shown in Fig. 1. A tabulation of typical operating voltages and currents along with the operating temperatures are shown in Table I. In turning on the source from a cold start, the ionizer, flange, and feed-tube heaters are turned on first. When the flange and feed-tube thermocouples indicate a temperature greater than  $\sim 400^{\circ}\text{C}$  and the ionizer is approximately  $1200^{\circ}\text{C}$ , the boiler is turned on. This turn-on sequence insures that the cesium vapor pressure is determined by the liquid vapor interface in the reservoir rather than a cold spot downstream of the reservoir. In turning off, the reverse procedure is followed.

TABLE I  
Tabulation of Typical Operating Parameters

Supply	Current, A	Voltage, V	Temperature, $^{\circ}\text{C}$
Ionizer Heater	2.9	9.0	1200
Flange Heater	5.0	2.5	480
Feed Tube Heater	3.2	6.0	450
Boiler Reservoir	3.5	5.8	300 to 425

T1192

a. Perveance Measurements - As described in the Phase I summary report, the theoretical design perveance for the Pierce geometry used for the cesium ion source is  $2.02 \times 10^{-11} \text{ A/V}^{3/2}$ . This line has been plotted in Fig. 2 along with experimentally measured points taken at three different boiler temperatures. Operation of this ion extraction system in the space charge-limited mode produces a

X = THERMOCOUPLE LOCATIONS

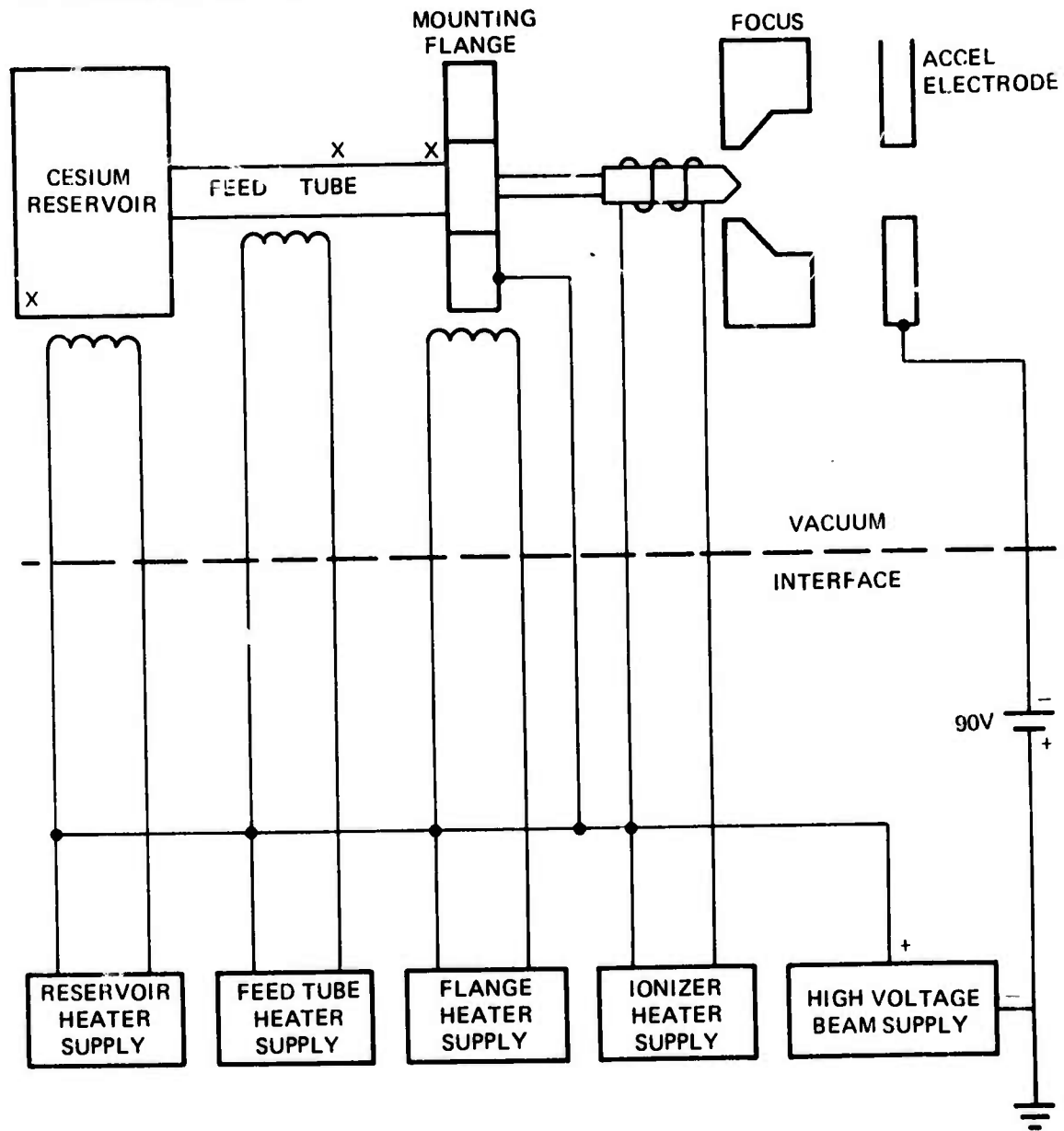


Fig. 1. Schematic of circuit diagram used for testing cesium ion source.

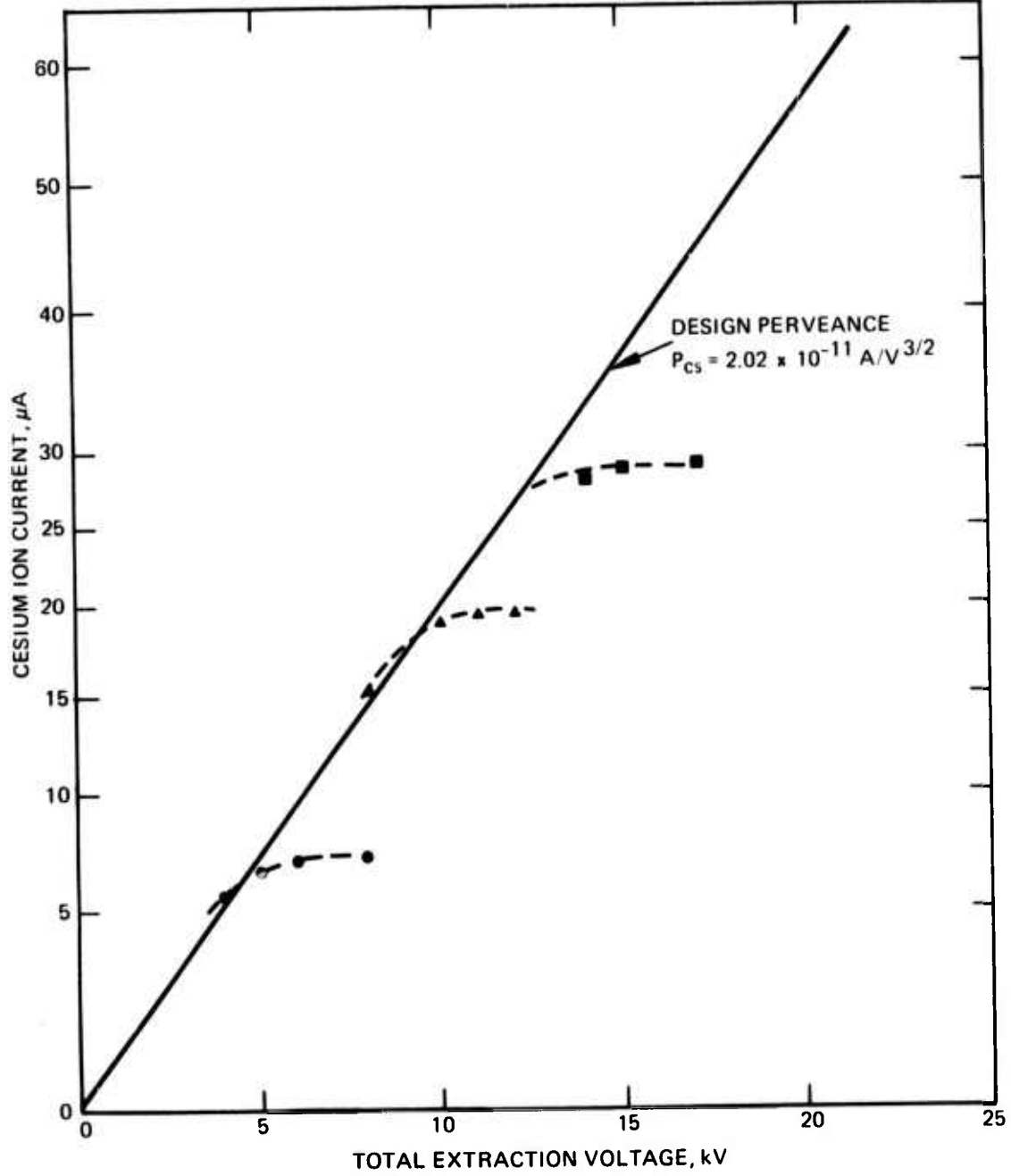


Fig. 2. Theoretical ion perveance line and experimental points.

beam current which varies as the extraction voltage to the 3/2 power. The design is such that identical trajectories would be obtained by operating at any point on the perveance line. The experimental observation that measured perveance points agrees closely with the theoretical value indicating that the calculated ion trajectories were actually achieved in the cesium ion source. A further verification of the beam quality is the fact that no sputter erosion was observed in the vicinity of the accelerator aperture. The experimental perveance points also show the flow-limited behavior expected when the cesium flow rate is limiting the current to less than the space charge limited value. This is analytically illustrated in Fig. 3 which shows how the ion trajectories can vary from their space charge limited counterparts under partial space charge operation. These trajectories show that it is desirable to operate as close as possible to the perveance line to achieve the most parallel beam (maximum brightness).

b. Measurement of Ion Source Brightness (Ref. 2 p 10-19, Phase I report) - We wish to determine the brightness of the extracted ion beam. To achieve the required high brightness, the source employs a long focus extraction system which produces a rather large external crossover of ~1-mm diam of which only the central region of ~0.1 mm is expected to demonstrate the high design brightness. The current density  $J_A$  at the 0.1-mm aperture will be almost constant and equal to the maximum value of the gaussian distribution in the crossover. By measuring the divergence angle of the apertured beam  $\alpha$ , an average brightness can be determined using

$$B = \frac{J_A}{\pi \alpha^2}$$

where

$$J_A = \frac{I}{A_h}$$

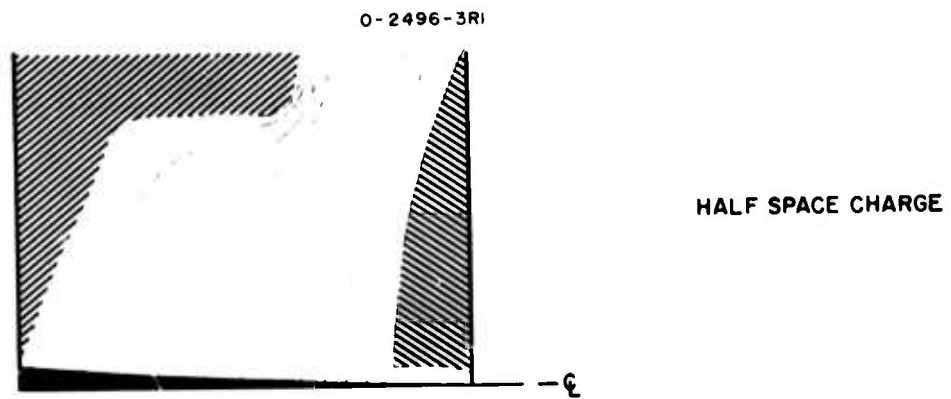
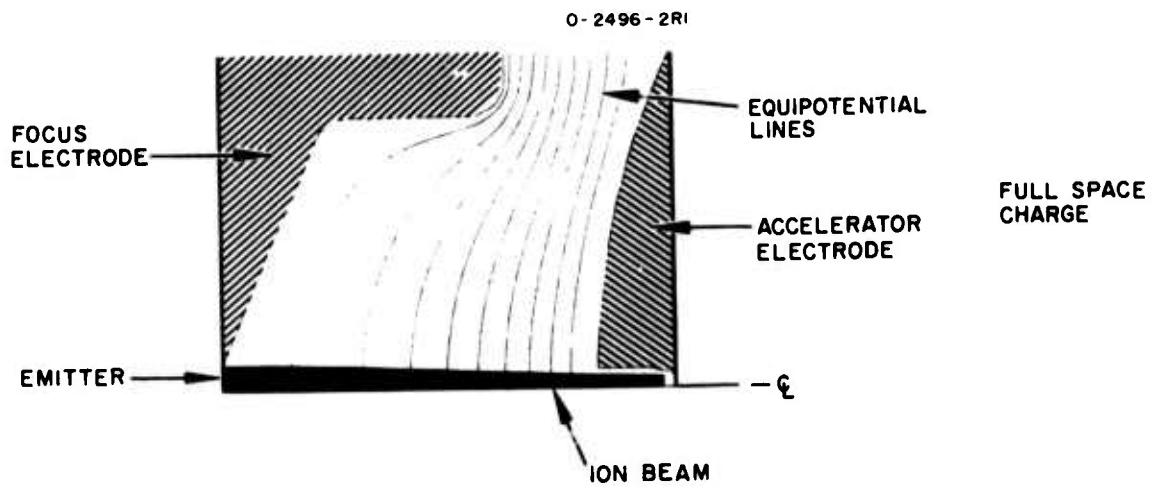


Fig. 3. Computer calculated trajectories for Pierce extraction geometry showing difference between half and full space charge operation.

and  $I$  is the current passing through a 0.1-mm diam aperture of area  $A_h$ .

The brightness measurement involves the measurement of a current and a beam angle. This is a difficult measurement for high-brightness narrow-angle sources because of the extreme alignment accuracy required. For example, alignment of two apertures to  $\sim 0.4$  mrad (equivalent to 5% of a nominal beam half angle of  $\sim 8$  mrad) requires transverse alignment accuracies of  $\sim 0.001$  cm for an aperture separation of 2.5 cm. Even more difficult is the angular alignment of the complete gun assembly with respect to the downstream apertures when the same degree of angular tolerances are required over appreciably greater distances.

In order to completely eliminate the alignment problems associated with the two-aperture method described above, the following method was used for the brightness measurement. A thin (0.001-cm thick) copper foil was placed 2.5 cm downstream from a 0.05-cm thick copper plate with a 0.013-cm diam defining aperture. In the order of minutes, a hole was sputtered through the thin copper foil. The current through this hole was then measured with a stationary Faraday cup with a 0.6-cm diam aperture. Post-test examination of this foil with an optical microscope was used to determine the diameter of the sputtered hole. A schematic of this experimental arrangement is shown in Fig. 4. The geometry of Fig. 5 shows how the brightness is calculated from the measured parameters.

$$\alpha_{\max} = \frac{r_o + r_1}{d}, \quad J_o = \frac{I_{\text{cup}}}{\pi r_o^2}$$

$$B_{\text{meas}} = \frac{J_o}{\pi \alpha_{\max}^2}, \quad B_{\text{theor}} = \frac{J_{\text{cath}}}{\pi} \frac{eV}{kT}$$

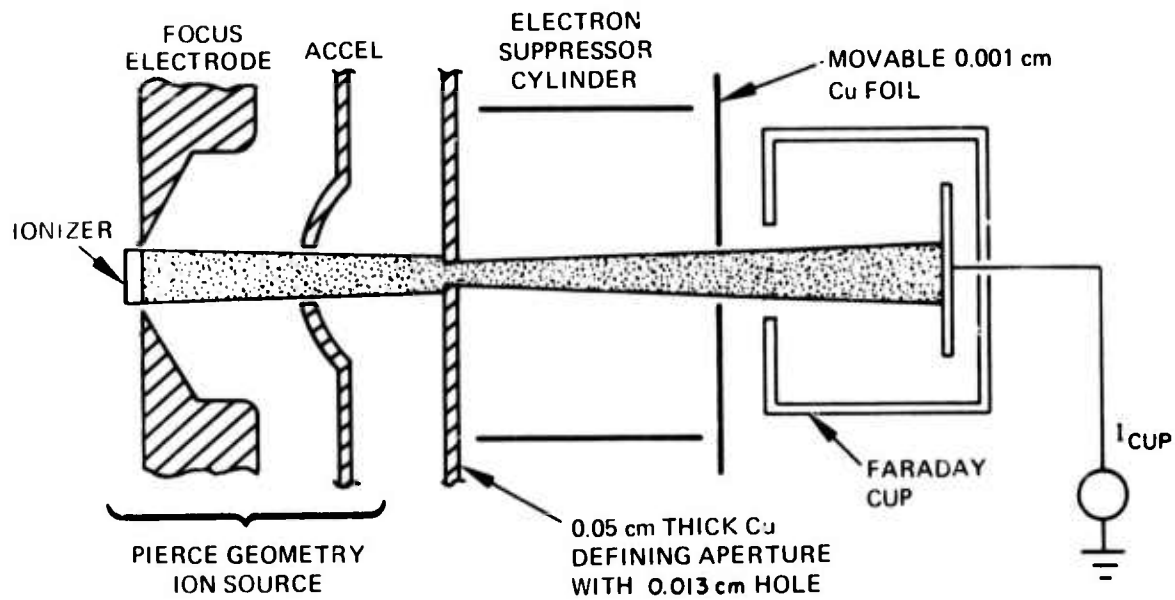


Fig. 4. Schematic of experimental arrangement used for making brightness measurements.

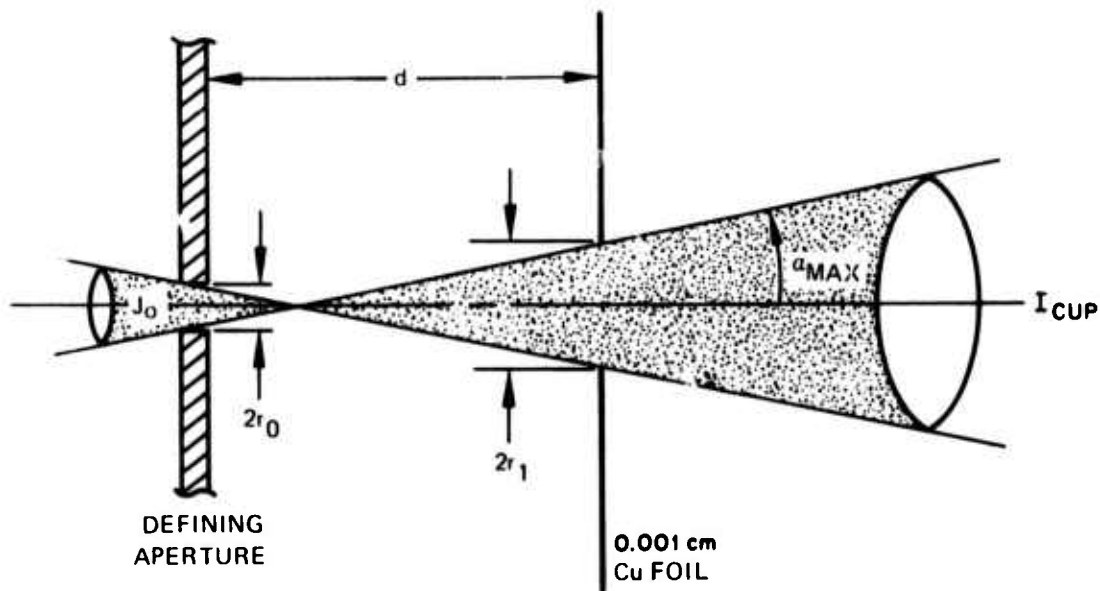


Fig. 5. Schematic showing how beam brightness is calculated from measured parameters.

Note that this method has the following features.

1. Self-aligning
2. Measurements made over a short enough distance so that space charge effects are negligible
3. Unambiguous current measured
4. Placed downstream a short distance where the current densities and currents are high.

With this method it is only necessary to finish sputtering the hole in the thin target foil before any enlargement takes place in the 0.01-cm hole in the aperture plate. This was insured in these experiments by monitoring the intercepted current on the aperture plate. Any enlargement of this hole was detected by a decrease in this intercepted current, which did not take place during the 10 to 20 min it typically took to sputter through the thin foil. During these experiments the aperture plate lasted anywhere from one to two hours at which time the intercepted current decreased from its steady-state value to essentially zero in the order of a few minutes.

A summary of the brightness measurements are tabulated in Table II. It is seen that there is good agreement between the measured and calculated brightness values for all except Case 2. When these points are plotted against voltage (see Fig. 6) it is seen the experimental points extrapolate to the brightness of  $200\text{A}/\text{cm}^2\text{-sr}$  for the full power conditions of 20 kV and  $57\ \mu\text{A}$ . It was impossible to measure the brightness by this technique at full beam current because back-sputtered copper from the aperture plate was depositing on the porous tungsten ionizer too rapidly. The calculations in Table II show this to be the case. Assuming a cosine distribution of sputtered atoms from the aperture plate, the arrival rate at the ionizer  $\Gamma_i$  is related to the sputtering rate,  $\Gamma_o$  at the aperture as follows:

$$\Gamma_i = \Gamma_o \cos \theta / \left( \frac{d}{r_o} \right)^2 \text{ atoms}/\text{cm}^2\text{-s}$$

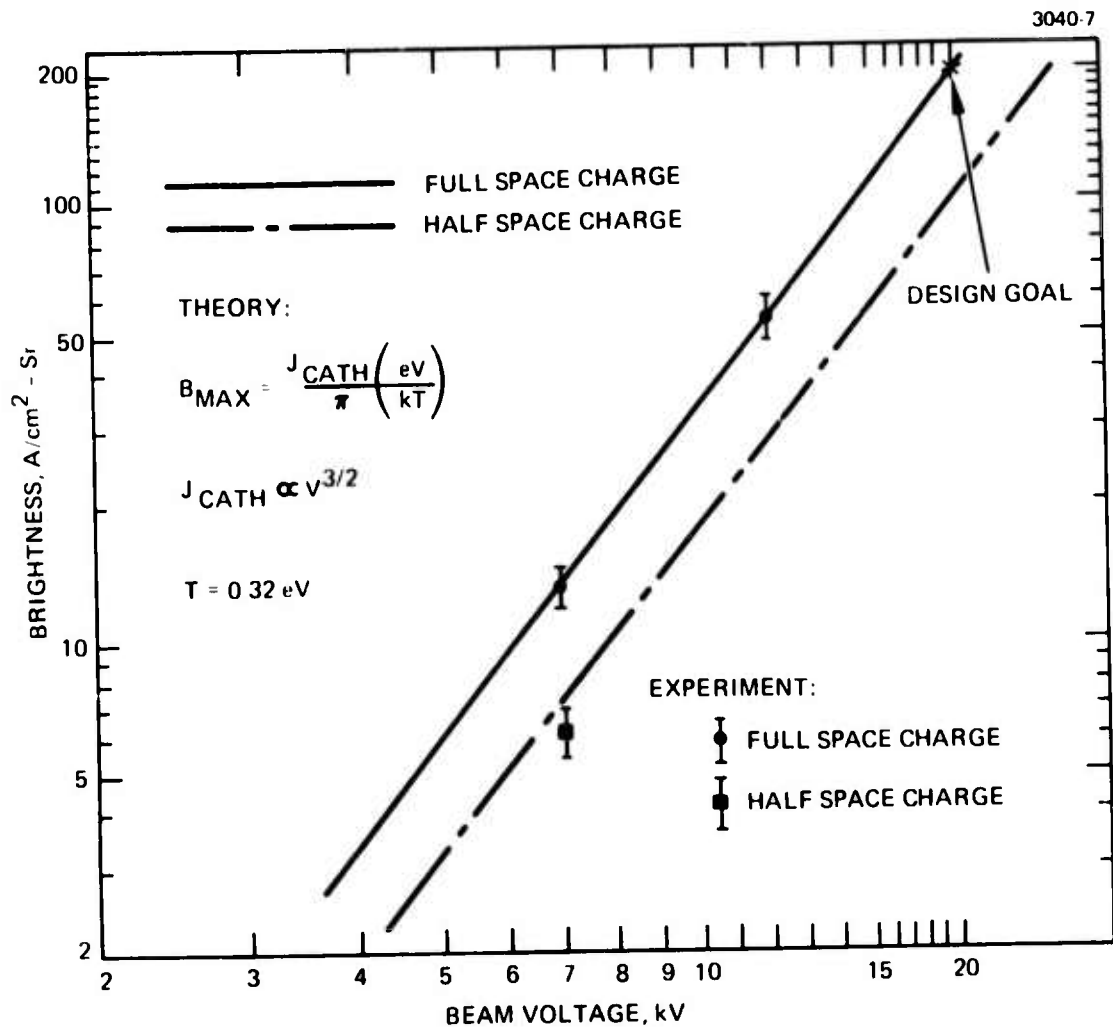


Fig. 6. Measured brightness values as a function of beam voltage.

TABLE II  
Summary of Parameters Measured During  
Brightness Experiments

$d = 2.54 \text{ cm}$
$2r_o = 0.013 \text{ cm}$
$kT = 0.32 \text{ eV}$

Case	$V_{+}$ kV	$I_{+}$ $\mu\text{A}$	$J_{\text{cath}}$ $\text{mA}/\text{cm}^2$	$I_{\text{cup}}$ $\mu\text{A}$	$2r_1$ cm	$\alpha_{\text{max}}$ mrad	$B_{\text{meas}}$ $\text{A}/\text{cm}^2\text{-sr}$	$B_{\text{theor}}$ $\text{A}/\text{cm}^2\text{-sr}$
1	7	6	1.05	0.40	0.053	13	5.98	7.37
2	12.5	9	2.81	0.42	0.048	12	7.37	19.7
3	7	13	2.28	0.006	0.004	3.25	15.8	15.96
4	12	30	5.26	0.136	0.008	4	59.2	62.7

where  $d$  is the distance between the aperture and ionizer (1.7 cm) and  $2r_o$  is the beam diameter at the aperture plate, (taken as 0.61 cm from post tests measurements of the enlarged aperture plate).

At a measured beam current of 30  $\mu\text{A}$  (case 4) the efflux of sputtered Cu atoms is given by

$$\Gamma_o = \left( \frac{J_{\text{aperture}}}{e} \right) S \text{ atoms}/\text{cm}^2\text{-s}$$

where  $S$  is the sputtering rate (taken as 12) and  $e$  is the electronic charge ( $1.6 \times 10^{-19} \text{ C}$ ). Thus

$$\Gamma_o = \left( \frac{I_{\text{aperture}}}{A} \right) \frac{S}{e}$$

$$\Gamma_o = 7.7 \times 10^{17} \text{ atoms}/\text{cm}^2\text{-s}$$

The arrival flux at the ionizer (for  $\cos \theta \approx 1$ ) is given by

$$\Gamma_i \approx \Gamma_o / \left( \frac{d^2}{r_o} \right) = 2.5 \times 10^{14} \text{ atoms/cm}^2\text{-s}$$

The above value is indeed in the region where the ionizer work function can be lowered. Reference to Fig. 7 shows that a copper arrival rate of greater than approximately  $10^{14}$  atoms/cm<sup>2</sup>-sec can contaminate the ionizer surface by lowering the surface work function.

## B. Iodine Negative Ion Source

### 1. Experimental Apparatus

The principle goal in the development of the negative ion source is that the source have a brightness value of  $100 \text{ A/cm}^2\text{-sr}$ . Based on the analysis presented in the Phase I Progress Report, this establishes a requirement that the source operate at a negative ion current density of  $5 \text{ mA/cm}^2$  with an electron to negative ion ratio of 500 or less. The efforts in this phase of the program were directed to develop a source which would achieve these operating levels.

The negative ion source was designed to use essentially the same ion-optics system as was used in the cesium ion source (see Phase I Report). The only significant modification is that the focus electrode must be operated at a negative potential with respect to the emitter surface so as to prevent any electron or ion current flow to the focus electrode. As a result, the focus electrode surface is located slightly to the rear of the emitter surface. This position was established by means of a computer analysis. The second distinction is that the emitter is a solid surface which is front fed by means of a molecular beam iodine gas source.

The emitter is fabricated from a sintered  $\text{LaB}_6$  rod. The  $\text{LaB}_6$  is machined to form a 0.084-cm diam cylinder. The cathode is shaped to minimize conductive heat loss, and is brazed into a

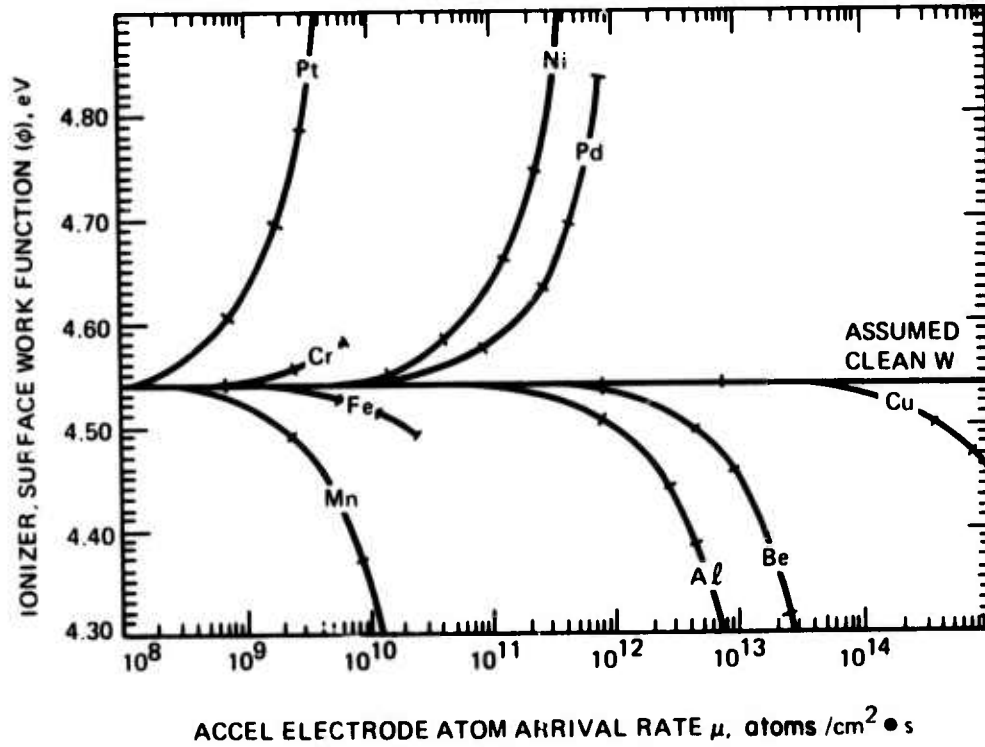


Fig. 7. Change in tungsten work function as a function of arrival rate for different metals.

molybdenum support structure. The  $\text{LaB}_6$  cathode is heated by means of a spiral wound tungsten heater. Both radiation and electron bombardment heating is used. This assembly is surrounded by a series of tungsten foil heat shields.

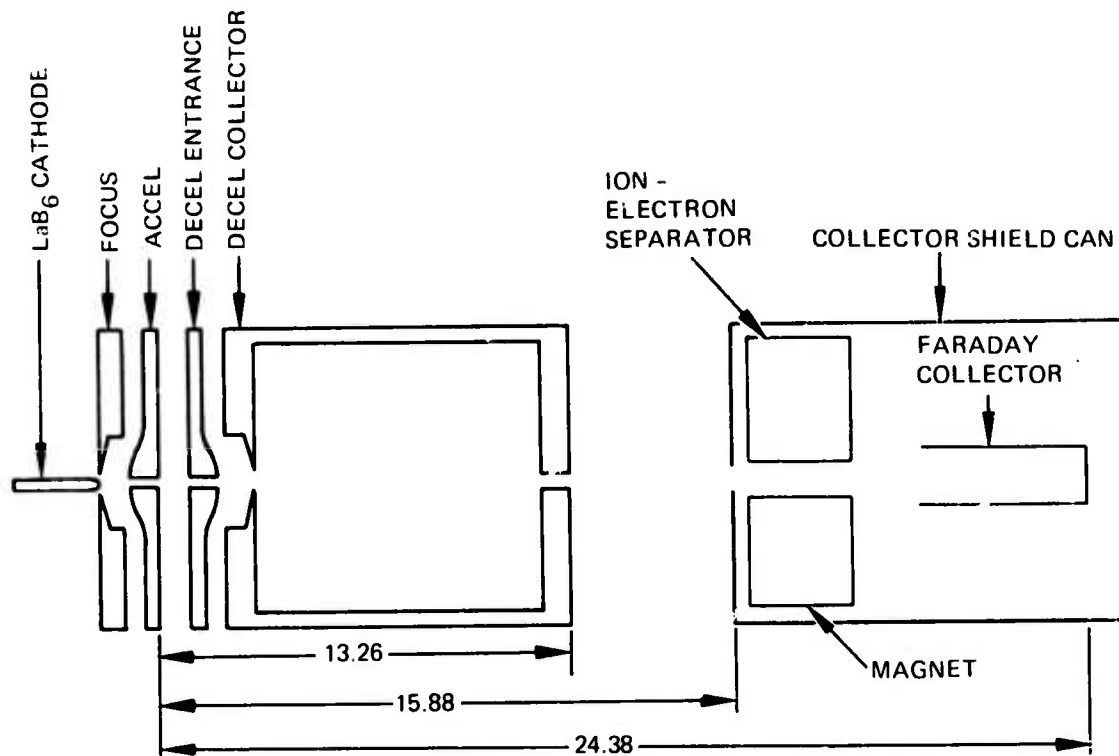
The iodine gas source consists of a temperature controlled reservoir of iodine. This is attached to a feed line which penetrates the accelerator electrode. The molecular beam of iodine gas is directed at the front face of the  $\text{LaB}_6$  cathode. The reservoir temperature is measured by means of an iron constantan thermocouple.

The ion and electron beam is directed into a massive copper collector (see Fig. 8). A portion of the beam travels through a 0.127-cm diameter orifice located 13.26 cm from the accel electrode. This beam enters the separator can through a 0.274-cm diameter orifice located 15.88 cm from the accel electrode. Inside this can a 3.18-cm diameter electromagnet is used to separate the electron and ion beams. A 0.617-cm diameter Faraday collector is used to monitor these currents. The electron-ion currents to all components in the system are measured as shown in Fig. 9.

The cathode temperature is determined by means of a micro optical brightness pyrometer. Temperatures are corrected for emissivity and window factors. The  $\text{LaB}_6$  surface is assigned an emissivity value of 0.6. The temperature measurements are made a point about 0.025 cm from the front surface of the cathode.

Because of the chemical reactivity of both iodine and  $\text{LaB}_6$ , special attention was given to the selection of materials for use in the apparatus. The potential problems are as follows:

- a. The reaction of iodine and metals to form a volatile compound which can then be decomposed on high-temperature surfaces and, thus, deposit a metal film on those surfaces. This reaction is used in the quartz-iodine lamps.
- b. The boron diffusion from  $\text{LaB}_6$  to metals in contact with high temperature  $\text{LaB}_6$ . This results in the decomposition of the  $\text{LaB}_6$ .



ACCEL ORIFICE = 0.076 cm DIAM  
 DECEL COLLECTOR EXIT = 0.127 cm DIAM  
 COLLECTOR SHIELD ENTRANCE = 0.274 cm DIAM  
 FARADAY COLLECTOR = 0.617 cm DIAM

Fig. 8. Cross-sectional view of negative ion system.

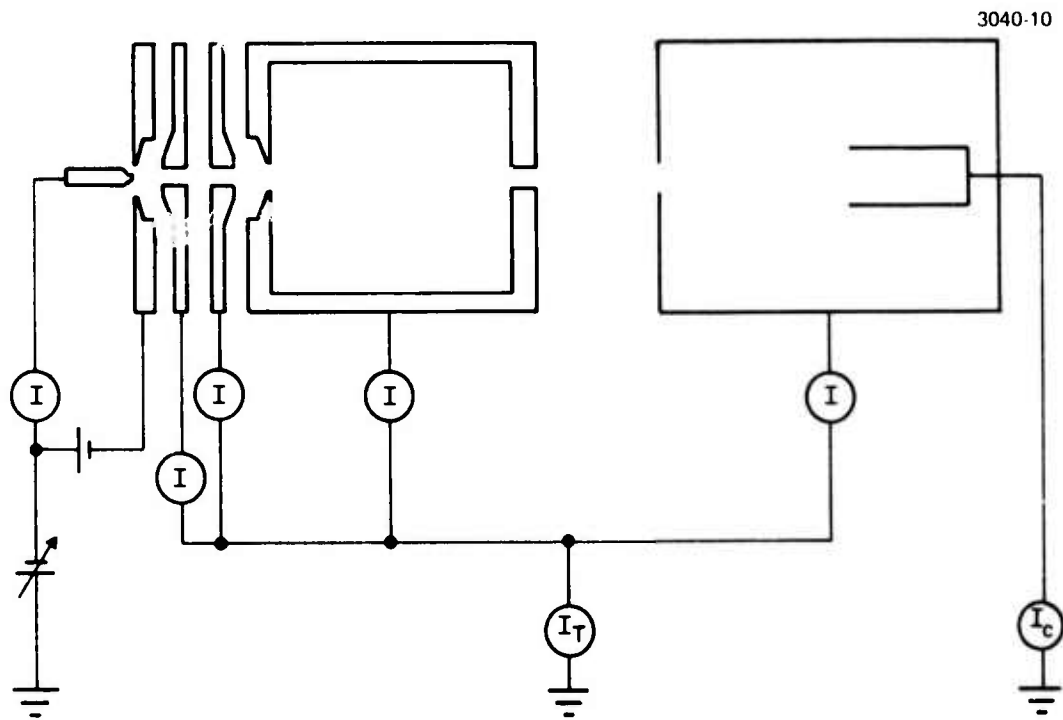


Fig. 9. Pictorial schematic of negative ion system.

Material compatibility studies were performed. They confirmed the problem of iodine reactivity at low temperatures. As a consequence, the iodine gas source was fabricated from fused quartz. The  $\text{LaB}_6$  cathode was designed so that the heat conduction to the base was limited. Thus, the attachment point at the base was held at a low enough temperature to minimize boron diffusion.

## 2. Experimental Results

The first effort in the program was to activate the  $\text{LaB}_6$  cathode and then to establish the operation of the cathode and the source electron-optics in the absence of iodine vapor. The electron emission exhibited a Richardson work function of 2.9 eV. This value is within the range of values reported in previous literature. The effective work functions were measured and found to be in agreement with the range of values quoted for  $\text{LaB}_6$ .

The initial efforts to measure the source perveance demonstrated the importance of exact positioning of the cathode surface. The source exhibited an anomalous cutoff at low potential which was traced to the fact that the cathode was located about 0.012 cm behind the design position. After adjustment, the source exhibited the design perveance. The very low accelerator currents indicated that the source was operating in the mode predicted by computer modeling (see Phase I Report).

After completion of these tests, the iodine reservoir was filled and the negative ion tests were begun. The results of the Phase I tests were confirmed and extended to higher values of ion current density.

The plots of the log of negative ion current versus reciprocal temperature of the cathode were linear indicating that the ionization process was described by the Saha-Langmuir expression. A typical plot is shown in Fig. 10.

The electron to ion ratios were measured for a number of source parameters. This value appears to be sensitive to the

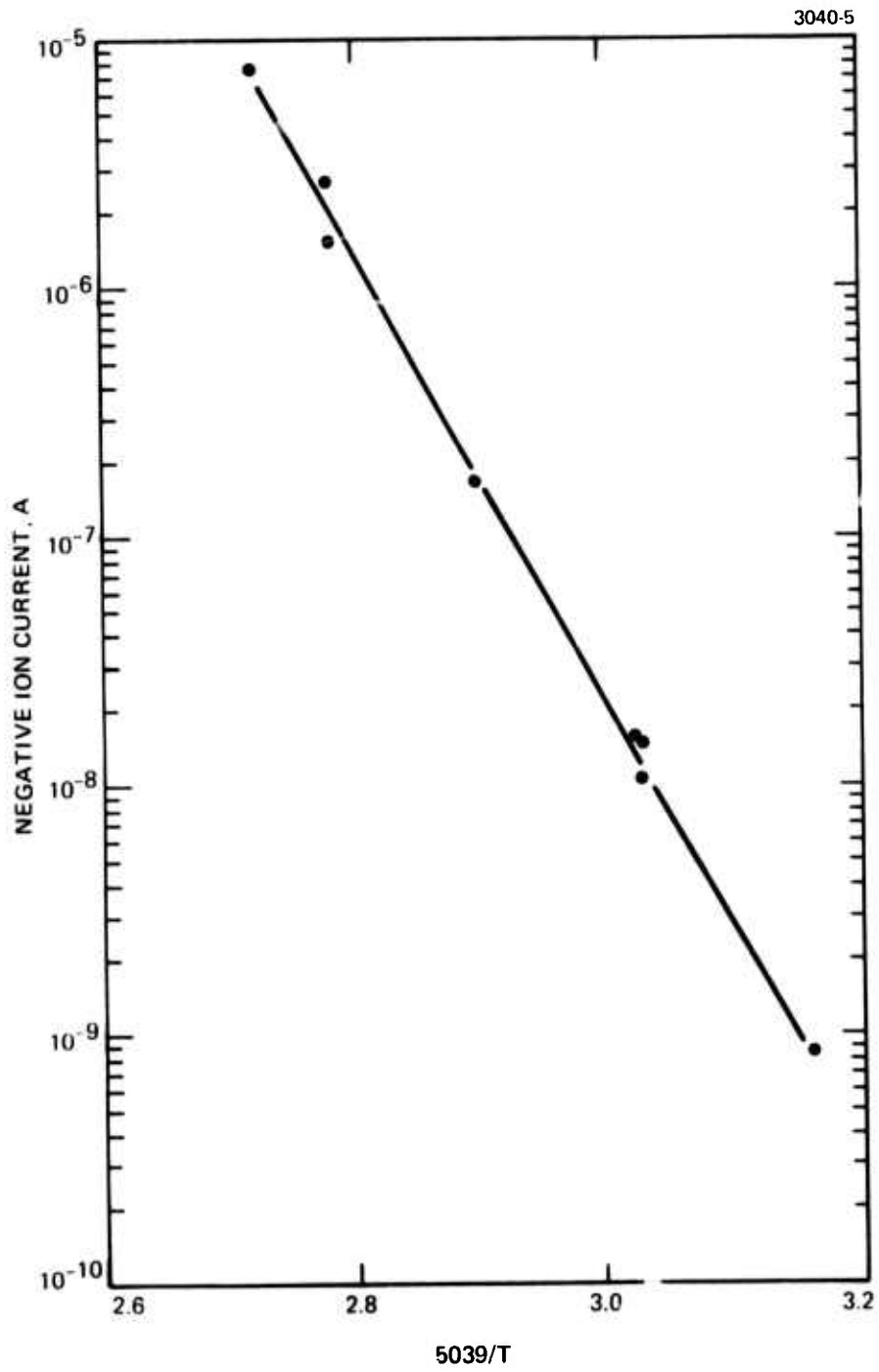


Fig. 10. Plot of negative ion current as a function of the reciprocal temperature of the emitter.

source temperature. As seen in Fig. 11, the observed values range from about 10 to about 250 for a wide range of temperatures and for varied iodine gas arrival rates. These values are within the desired ranges.

The ion current density was calculated based on the total emission of the cathode. The overall electron current density was used to determine the effective emitting area and, thus, to measure the ion current density at the source. The observed values ranged about the design goal of  $5 \text{ mA/cm}^2$ .

An estimate of the negative ion source brightness was made using the exit apertures of the accel electrode and the decel collector to define the beam geometry. The brightness values were about 50 to  $70 \text{ A/cm}^2\text{-sr}$ , which nearly meets the contract specifications.

Note - The large quantity of numerical data collected during the iodine/LaB<sub>6</sub> experiments are currently undergoing analysis and will be forwarded to the AFTAC Project Manager for approval to publish as a separate report in a scientific journal.

### C. System Design

A system design was presented in the Phase I report of this contract. As a result of discussion with the AFTAC program manager and the ultimate user of the AMS system (General Electric Co) a number of design modifications have been suggested. This design will be finalized by the end of the third month of the Phase III program and a detailed design submitted at that time.

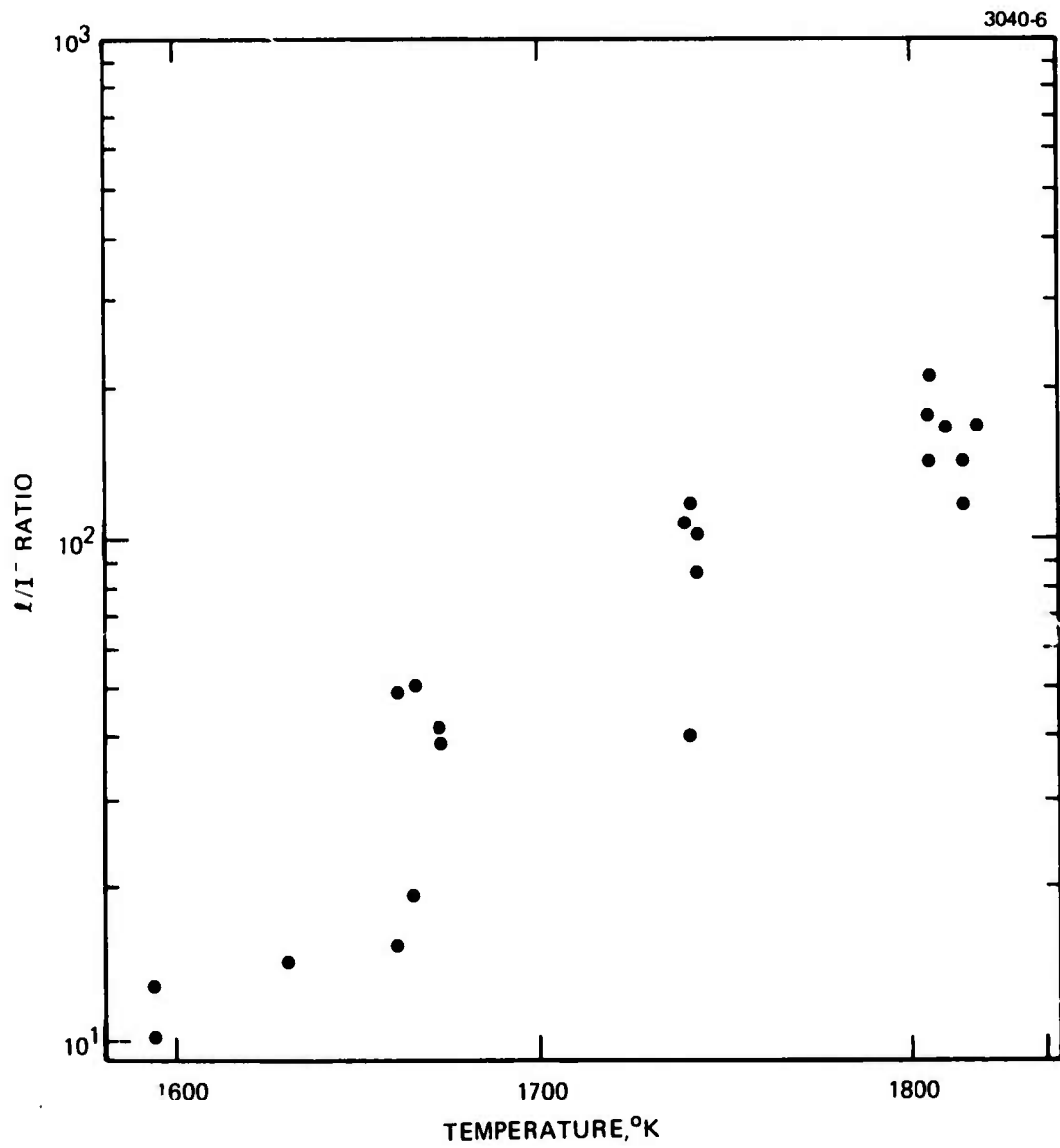


Fig. 11. Plot of electron to ion ratio values as a function of emitter temperature.

#### IV. CONCLUSION AND SUMMARY

The experiments conducted during Phase II have verified the accuracy of the ion-optical design calculations and the ability to effectively produce negative iodine ions on a lanthanum hexaboride surface. These are the two fundamental requirements for meeting the contractual brightness specifications.

## REFERENCES

1. G. R. Brewer, Ion Propulsion, Gordon and Breach (1970).
2. H. King, "Advanced Ion Source," Phase I Report, Contract F08606-73-C-0038.